Cyanate Ester/Polyhedral Oligomeric Silsesquioxane (POSS) Nanocomposites: Synthesis and Characterization†

Kaiwen Liang,‡ Guizhi Li,§ Hossein Toghiani,‡ Joseph H. Koo,|| and Charles U. Pittman, Jr.*,§

Dave C. Swalm School of Chemical Engineering, Mississippi State University, Mississippi State, Mississippi 39762, Department of Chemistry, Mississippi State University, Mississippi State, Mississippi 39762, and Department of Mechanical Engineering, Texas A&M University, College Station, Texas 78712

Received July 19, 2005

Cyanate ester (PT-15, Lonza Corp.) composites containing the blended polyhedral oligomeric silsesquioxane (POSS), TriSilanolPhenyl-POSS ($C_{42}H_{38}O_{12}Si_7$), were prepared containing PT-15/POSS 99/1, 97/3, 95/5, 90/10, and 85/15 w/w ratios. The composites were characterized by FT-TR, X-ray diffraction (XRD), small-angle neutron scattering (SANS), scanning electron microscopy (SEM), X-ray energy dispersive spectroscopy (X-EDS), transmission electron microscopy (TEM), dynamic mechanical thermal analysis (DMTA), and three-point bending flexural tests. TriSilanolPhenyl-POSS was throughly dispersed into uncured liquid PT-15 resin. After curing, XRD, SANS, and X-EDS measurements were consistent with partial molecular dispersion of a portion of the POSS units in the continuous matrix phase while the remainder forms POSS aggregates. Larger aggregates are formed at higher loadings. SANS, SEM, and TEM show that POSS-enriched nanoparticles are present in the PT-15/POSS composites. The storage bending moduli, E', and the glass transition temperatures, T_g, of PT-15/POSS 99/1, 97/3, and 95/5 composites are higher than those of the pure PT-15 over the temperature range from 35 to 350 °C. The E' values for all these composites (except for the 15 wt % POSS sample) are significantly greater than that of the pure resin at $T > T_g$. Therefore, small amounts (≤5 wt %) of TriSilanolPhenyl-POSS incorporated into cyanate ester resin PT-15 can improve the storage modulus and the high-temperature properties of these cyanate ester composites versus the pure PT-15 resin. The flexural strength and flexural modulus are also raised by POSS incorporation.

Introduction

The development of hybrid organic polymer−inorganic nanocomposites with a variety of new and improved properties has attracted much research interest in the past few years.[1] The inorganic nanophases being studied include nanoclays,[2] carbon nanotubes,[3] vapor-grown carbon nanofibers,[4] various inorganic nanofibers,[5] and polyhedral oligomeric silsesquioxanes.[1s−z,6] Silsesquioxane is the term for all structures with the formula $(RSiO_{1.5})_n$, where R is hydrogen or any alkyl, alkylene, aryl, arylene, or organofunctional derivative of alkyl, alkylene, aryl, or arylene groups. Silsesquioxanes may form ladder,[7] cage,[7a,8] partial cage,[9] and polymer structures.[1z,10] Among various types of silsesquioxanes, polyhedral oligomeric silsesquioxanes (POSS) reagents offer a unique opportunity for preparing hybrid organic−inorganic materials with the inorganic structural units truly molecularly dispersed within the nanocomposites. Typical POSS cages have the empirical formulas $(RSiO_{1.5})_{8,10,or12}$. These are referred to as T_8, T_{10}, and T_{12} cages, respectively. Each cage silicon atom is attached to a single R substituent and these substituents can be organic (cyclohexyl, phenyl, etc.) or inorganic−organic hybrids (e.g., −$OSiMe_2OPh$). Incompletely closed cage structures are also possible. Two sample POSS structures, both a T_8 cage and an incompletely closed cage molecule **1** are shown below. POSS nanostructured chemicals, with sizes from 1 to 3 nm in diameter, can be thought of as the smallest possible particles of silica. However, unlike silica, silicones, or fillers, each POSS molecule contains either nonreactive or reactive organic substituents at the corner silicon atoms. These organic substituents can make these POSS molecules compatible with polymers or monomers.

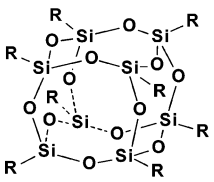

T_8 POSS cage

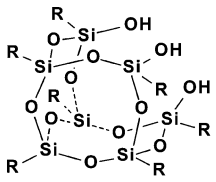

1 (R = Phenyl)

Partial T_8 cage with one corner Si missing ($C_{42}H_{38}O_{12}Si_7$)

POSS derivatives are now available with reactive functionalities suitable for polymerization or grafting.[1s−z,6,11] Hence, POSS nanostructured chemicals can be incorporated into common plastics via copolymerization,[11c,12] grafting,[11c,13] or blending,[11c,13,14] thereby offering a special opportunity for the preparation of new thermoset[6,15] and thermoplastic

† This work is taken from the Ph.D. dissertation of Kaiwen Liang.

* Corresponding author. E-mail: cpittman@ra.msstate.edu.

‡ Dave C. Swalm School of Chemical Engineering, Mississippi State University.

§ Department of Chemistry, Mississippi State University.

|| Texas A&M University, current address: Department of Mechanical Engineering, University of Texas at Austin, Austin, TX 78712.

10.1021/cm051582s CCC: $33.50
Published on Web 12/18/2005

materials.[1v,z,12b,c,13,14,16] The incorporation of POSS derivatives into polymeric materials can lead to substantial improvements in polymer properties including increases in use temperature,[17] oxidation resistance,[13] surface hardening,[13] and mechanical properties,[18] as well as reductions in flammability,[19] heat evolution,[20] and viscosity[21] during processing. These improvements have been shown to apply to a wide range of thermoplastics and thermoset systems, i.e., methacrylates,[22] styrenes,[23] norbornenes,[24] ethylenes,[25] epoxies,[26] siloxanes,[12c] etc.

Cyanate esters are currently in widespread use because of their high thermal stability, excellent mechanical properties flame resistance, low outgassing, and radiation resistance.[27] Applications of cyanate ester include structural aerospace, electronic, microwave-transparent composites, encapsulants, and adhesives. Cyanate ester resins are superior to conventional epoxy, polyimide, and BMI resins. For example, the moisture absorption rate of cyanate esters is lower than those of epoxy, polyimide, and BMI resins. High glass transition temperatures (>250 °C) of cyanate esters fill a temperature

(1) (a) Giannelis, E. P. *Adv. Mater.* **1996**, *8*, 29−35. (b) Jog, J. P.; Hambir, S.; Bulakh, N. *Polym. Eng. Sci.* **2002**, *42*, 1800−1807. (c) Kim, D. S.; Lee, K. M. *J. Appl. Polym. Sci.* **2003**, *90*, 2629−2633. (d) Liu, Z. J.; Chen, K. Q.; Yan, D. Y. *Eur. Polym. J.* **2003**, *39*, 2359−2366. (e) Priya, L.; Jog, J. P. *J. Polym. Sci., Part B: Polym. Phys.* **2002**, *40*, 1682−1689. (f) Wang, Y. Z.; Zhang, L. Q.; Tang, C. H.; Yu, D. S. *J. Appl. Polym. Sci.* **2000**, *78*, 1879−1883. (g) Bureau, M. N.; Denault, J.; Cole, K. C.; Enright, G. D. *Polym. Eng. Sci.* **2002**, *42*, 1897−1906. (h) Wan, C. Y.; Qiao, X. Y.; Zhang, Y.; Zhang, Y. X. *Polym. Test.* **2003**, *22*, 453−461. (i) Wu, S. H.; Wang, F. Y.; Ma, C. C. M.; Chang, W. C.; Kuo, C. T.; Kuan, H. C.; Chen, W. J. *Mater. Lett.* **2001**, *49*, 327−333. (j) Burnside, S. D.; Giannelis, E. P. *Chem. Mater.* **1995**, *7*, 1597−1600. (k) Agag, T.; Koga, T.; Takeichi, T. *Polymer* **2001**, *42*, 3399−3408. (l) Kodgire, P.; Kalgaonkar, R.; Hambir, S.; Bulakh, N.; Jog, J. P. *J. Appl. Polym. Sci.* **2001**, *81*, 1786−1792. (m) Chen, Z.; Gong, K. *J. Appl. Polym. Sci.* **2002**, *84*, 1499−1503. (n) Gilman, J. W. *Appl. Clay. Sci.* **1999**, *15*, 31−49. (o) Lepoittevin, B.; Devalckenaere, M.; Pantoustier, N.; Alexandre, M.; Kubies, D.; Calberg, C.; Jerome, R.; Dubois, P. *Polymer* **2002**, *43*, 4017−4023. (p) Gu, A. J.; Liang, G. Z. *Polym. Degrad. Stab.* **2003**, *80*, 383−391. (q) Bourbigot, S.; Devaux, E.; Flambard, X. *Polym. Degrad. Stab.* **2002**, *75*, 397−402. (r) Gilman, J. W.; Kashiwagi, T.; Lichtenhan, J. D. *SAMPE J.* **1997**, *33*, 40−46. (s) Romo-Uribe, A.; Mather, P. T.; Haddad, T. S.; Lichtenhan, J. D. *J. Polym. Sci., Part B: Polym. Phys.* **1998**, *36*, 1857−1872. (t) Mather, P. T.; Jeon, H. G.; Romo-Uribe, A.; Haddad, T. S.; Lichtenhan, J. D. *Macromolecules* **1999**, *32*, 1194−1203. (u) Lee, A.; Lichtenhan, J. D. *J. Appl. Polym. Sci.* **1999**, *73*, 1993−2001. (v) Jeon, H. G.; Mather, P. T.; Haddad, T. S. *Polym. Int.* **2000**, *49*, 453−457. (w) Fu, B. X.; Hsiao, B. S.; Pagola, S.; Stephens, P.; White, H.; Rafailovich, M.; Sokolov, J.; Mather, P. T.; Jeon, H. G.; Phillips, S.; Lichtenhan, J. D.; Schwab, J. *Polymer* **2001**, *42*, 599−611. (x) Gonzalez, R. I.; Phillips, S. H.; Hoflund, G. B. *J. Spacecr. Rockets* **2000**, *37*, 463−467. (y) Lichtenhan, J. D.; Otonari, Y. A.; Carr, M. J. *Macromolecules* **1995**, *28*, 8435−8437. (z) Haddad, T. S.; Lichtenhan, J. D. *Macromolecules* **1996**, *29*, 7302−7304.

(2) (a) Simon, S. L.; Gillham, J. K. *J. Appl. Polym. Sci.* **1993**, *47*, 461−485. (b) Yeh, J. M.; Chin, C. P. *J. Appl. Polym. Sci.* **2003**, *88*, 1072−1080. (c) Wang, Z.; Pinnavaia, T. J. *Chem. Mater.* **1998**, *10*, 1820−1826. (d) Alexandre, M.; Dubois, P. *Mater. Sci. Eng. R Rep.* **2000**, *28*, 1−63. (e) Gangun, S.; Dean, D. *Polymer* **2003**, *44*, 1315−1319. (f) Ganquli, S.; Dean, D.; Vaia, R. *Polym. Mater. Sci. Eng.* **2002**, *87*, 94−96.

(3) (a) Dufresne, A.; Paillet, M.; Putaux, J. L.; Canet, R.; Carmona, F.; Delhaes, P. *J. Mater. Sci.* **2002**, *37*, 3915−3923. (b) Penumadu, D.; Dutta, A.; Pharr, G. M.; Files, B. *J. Mater. Res.* **2003**, *18*, 1849−1853. (c) Thostenson, E. T.; Chou, T. W. *J. Phys. D: Appl. Phys.* **2002**, *35*, L77−L80. (d) Bai, J. B.; Allaoui, A. *Compos. Part A: Appl. Sci. Manuf.* **2003**, *34*, 689−694.

(4) (a) Kuriger, R. J.; Alam, M. K.; Anderson, D. P.; Jacobsen, R. L. *Compos. Part A: Appl. Sci. Manuf.* **2002**, *33*, 53−62. (b) Shofner, M. L.; Rodriguez-Macias, F. J.; Vaidyanathan, R.; Barrera, E. V. *Compos. Part A: Appl. Sci. Manuf.* **2003**, *34*, 1207−1217. (c) Kuriger, R. J.; Alam, M. K. *Polym. Compos.* **2001**, *22*, 604−612. (d) Gordeyev, S. A.; Ferreira, J. A.; Bernardo, C. A.; Ward, I. M. *Mater. Lett.* **2001**, *51*, 32−36. (e) Lakshminarayanan, P. V.; Toghiani, H.; Pittman, C. U., Jr. *Carbon* **2004**, *42*, 2433−2442. (f) Patton, R. D.; Pittman, C. U., Jr.; Wang, L. *Int. SAMPE Tech. Conf.* **1997**, *29*, 77−84. (g) Patton, R. D.; Pittman, C. U., Jr.; Wang, L.; Hill, J. R.; Day, A. *Compos. Part A: Appl. Sci. Manuf.* **2001**, *33*, 243−251.

(5) (a) Yamamoto, K.; Otsuka, H.; Takahara, A.; Wada, S. I. *J. Adhes.* **2002**, *78*, 591−602. (b) Xu, H. Y.; Kong, H.; Yang, Z. B. *Chin. J. Mater. Res.* **2003**, *17*, 127−131.

(6) Lee, A.; Lichtenhan, J. D. *Macromolecules* **1998**, *31*, 4970−4974.

(7) (a) Unno, M.; Suto, A.; Takada, K.; Matsumoto, H. *Bull. Chem. Soc. Jpn.* **2000**, *73*, 215−220. (b) Xie, P.; Zhang, R. *Polym. Adv. Technol.* **1997**, *8*, 649−656. (c) Xu, H.; Xie, P.; Zhang, R. *Eur. Polym. J.* **2001**, *37*, 2397−2405.

(8) (a) Lichtenhan, J. D. *Comments Inorg. Chem.* **1995**, *17*, 115−130. (b) Lichtenhan, J. D. *Polymeric Material Encyclopedia*; Salamone, J. C., Ed.; CRC Press: New York, 1996; Vol. 10, pp 7768−7778. (c) Feher, F. J.; Budzichowski, T. A. *Polyhedron* **1995**, *14*, 3239−3253.

(9) Deng, J.; Polidan, J. T.; Hottle, J. R.; Farmer-Creely, C. E.; Viers, B. D.; Esker, A. R. *J. Am. Chem. Soc.* **2002**, *124*, 15194−15195.

(10) Pyun, J.; Matyjaszewski, K.; Wu, J.; Kim, G. M.; Chun, S. B.; Mather, P. T. *Polymer* **2003**, *44*, 2739−2750.

(11) (a) Schwab, J. J.; Lichtenhan, J. D.; Chaffee, K. P.; Mather, P. T.; Romo-Uribe, A. *Mater. Res. Soc. Symp. Proc.* **1998**, *519*, 21−27. (b) Klein, L. C., Francis, L. F., DeGuire, M. R., Mark, J. E., Eds. *Organic/inorganic hybrid materials II. MRS Symposium Proceedings*, 1999; p 576. (c) Lichtenhan, J. D.; Schwab, J. J. *Int. SAMPE Tech. Conf.* **2000**, *32*, 185−191. (d) Li, G.; Wang, L.; Ni, H.; Pittman, C. U., Jr. *J. Inorg. Organomet. Polym.* **2001**, *11*, 123.

(12) (a) Mather, P. T.; Jeon, H. G.; Haddad, T. S. *Polym. Prepr.* **2000**, *41*, 528−529. (b) Haddad, T. S.; Choe, E.; Lichtenhan, J. D. *Mater. Res. Soc. Symp. Proc.* **1996**, *435*, 25−32. (c) Haddad, T. S.; Stapleton, R.; Jeon, H. G.; Mather, P. T.; Lichtenhan, J. D.; Phillips, S. H. *Polym. Prepr.* **1999**, *40*, 496−497.

(13) Phillips, S. H.; Blanski, R. L.; Svejda, S. A.; Haddad, T. S.; Lee, A.; Lichtenhan, J. D.; Feher, F. J.; Mather, P. T.; Hsiao, B. S. *Mater. Res. Soc. Symp. Proc.* **2000**, *628*, CC4.6.1−CC4.6.10.

(14) Blanski, R. L.; Phillips, S. H.; Chaffee, K.; Lichtenhan, J. D.; Lee, A.; Geng, H. P. *Polym. Prepr.* **2000**, *41*, 585−586.

(15) (a) Haddad, T. S.; Lee, A.; Mather, P. T.; Phillips, S. H. *Polym. Prepr.* **2000**, *41*, 584. (b) Lu, S.; Martin, G. C. *Conf. Proc./ANTEC* **2003**, *2*, 1893−1897. (c) Constable, G. S.; Coughlin, E. B.; Lesser, A. J. *Conf. Proc./ANTEC* **2003**, *2*, 1663−1667. (d) Li, G.; Wang, L.; Toghiani, H.; Pittman, C. U., Jr.; Daulton, T. L.; Koyama, K. *Macromolecules* **2001**, *34*, 8686−8693. (e) Li, G.; Wang, L.; Toghiani, H.; Daulton, T. L.; Pittman, C. U., Jr. *Polymer* **2002**, *43*, 4167−4176. (f) Gupta, S. K.; Schwab, J. J.; Lee, A.; Fu, B. X.; Hsiao, B. S. *Int. SAMPE Symp. Exhib.* **2002**, *47*, 1517−1526. (g) Feher, F. J.; Lucke, S.; Schwab, J. J.; Lichtenhan, J. D.; Phillips, S. H.; Lee, A. *Polym. Prepr.* **2000**, *41*, 526.

(16) (a) Haddad, T. S.; Mather, P. T.; Jeon, H. G.; Romo-Uribe, A.; Farris, A. R.; Lichtenhan, J. D. *Mater. Res. Soc. Symp.−Proc. V 519, Org./Inorg. Hybrid Mater.* **1998**, 381−386. (b) Mantz, R. A.; Jones, P. F.; Chaffee, K. P.; Lichtenhan, J. D.; Ismail, M. K.; Burmeister, M. *Chem. Mater.* **1996**, *8*, 1250−1259.

(17) (a) Xu, H. Y.; Kuo, S. W.; Lee, J. Y.; Chang, F. C. *Polymer* **2002**, *43*, 5117−5124. (b) Horwath, J.; Schweickart, D. *IEEE* **2002**, 644−647.

(18) (a) Pellice, S. A.; Fasce, D. P.; Williams, R. J. J. *J. Polym. Sci., Part B: Polym. Phys.* **2003**, *41*, 1451−1461. (b) Lee, A. *Mater. Res. Soc. Symp.−Proc.* **1999**, *576*, 343−350.

(19) Philips, S. H.; Gonzalez, R. I.; Chaffee, K. P.; Haddad, T. S.; Hoflund, G. B.; Hsiao, B. S.; Fu, B. X. *SAMPE* **2000**, *45*, 1921−1932.

(20) Huang, J. C.; He, C. B.; Xiao, Y.; Mya, K. Y.; Dai, J.; Siow, Y. P. *Polymer* **2003**, *44*, 4491−4499.

(21) Fu, B. X.; Namani, M.; Lee, A. *Polymer* **2003**, *44*, 7739−7747.

(22) Lichtenhan, J. D.; Otonari, Y. A.; Carr, M. J. *Macromolecules* **1995**, *28*, 8435.

(23) Haddad, T. S.; Lichtenhan, J. D. *Macromolecules* **1996**, *29*, 7302−7304.

(24) Bharadwaj, R. K.; Berry, R. J.; Farmer, B. L. *Polymer* **2000**, *41*, 7209−7221.

(25) Tsuchida, A.; Bolln, C.; Sernetz, F. G.; Frey, H.; Mulhaupt, R. *Macromolecules* **1997**, *30*, 2818.

(26) Lee, A.; Lichtenhan, J. D. *Macromolecules* **1998**, *31*, 4970−4974.

(27) (a) Simon, S. L.; Gillham, J. K. *J. Appl. Polym. Sci.* **1993**, *47*, 461. (b) Brand, R. A.; Harrison, E. S. *NASA CR* **1982**, 50. (c) Das, S.; Prevorsek, D. C.; Debona, B. T. *21st SAMPE Tech. Conf.* **1989**, *21*, 972. (d) McConnell, V. P. *Adv. Compos.* **1992**, *7*, 28. (e) Shimp, D. A.; Christenson, J. R.; Ising, S. J. *34th Int. SAMPE Symp.* **1991**, *36*, 336. (f) Snow, A. W.; Buckley, L. J.; Armistead, J. P. *J. Polym. Sci., Polym. Chem.* **1999**, *37*, 135−150. (g) Hamerton, I. *Chemistry and Technology of Cyanate Ester Resins*; Chapman &Hall: London, 1994.

regime intermediate between that of epoxy resins and the hazardous/difficult to handle polyimide or BMI resins. Cyanate ester resins are easy to process in a manner similar to epoxy resins. Cyanate esters undergo thermal or catalytic cyclotrimerization to form triazine rings during curing. We are studying cyanate esters as precursors to carbon−carbon materials because they may be cured without outgassing and they form dense thermally stable resins. However, cyanate esters tend to be brittle and have reduced impact resistance like most highly cross-linked thermosets.

The objective of this work is to incorporate nanosized silica phases into carbon−carbon materials. First, the nature of the dispersion after curing the resin needs to be understood. Can such nanodispersed phases be maintained upon pyrolysis of the cured cyanate ester resin/carbon cloth composite and the subsequent densification processes? If nanodispersed phases occur, as envisioned, will they function to form O_2 diffusion barriers and to serve as char-forming nuclei? The specific POSS compound, TriSilanolPhenyl-POSS, **1**, is used as the nanophase in this work. Will incorporating this nanophase improve some of the properties of the original cyanate ester resin matrix? Can molecular level dispersions of **1** within the cured cyanate ester resin be achieved or will aggregation/phase separation occur? If molecular level dispersion of **1** is achieved within the cured resin, this may lead to carbon−carbon composites with different properties than if phase-separated aggregates form. When POSS chemicals are blended with liquid resins, they may or may not be able to dissolve in the resin. Even when they are soluble, they may phase separate to varying degrees during resin curing as the entropy of mixing decreases.

This paper reports the blending of TriSilanolPhenyl-POSS, **1**, into cyanate ester resin (PT-15, Lonza Corp.), followed by thermal curing to determine the nature of cyanate ester/nanocomposites formed. POSS-**1** was selected because the three hydroxyl groups might aid solubility into PT-15 and we thought they might react with cyanate ester functions at high temperatures to aid dispersion.[28,29] Cyanate ester/**1** composites with compositions (w/w) of 99/1, 97/3, 95/5, 90/10, and 85/15 were made and examined to determine the extent of phase separation of POSS into particle aggregates versus the extent of compatible molecular dispersion. The effect of introducing POSS-**1** into this cyanate ester polymer system on dynamic mechanical properties and the thermal dimensional stability was also evaluated. Further work is underway to study these PT-15/**1** systems as the bonding matrix for carbon−carbon composite materials.

Experimental Section

Materials. The phenolic-derived cyanate ester resin, PT-15, used in this work was supplied by Lonza Inc. PT-15 is composed of cyanate esters derived from a bisphenol-F mixture of **2**−**4** with some larger molecules such as **5** included. Excess ClCN or BrCN converted all phenolic hydroxyls to OCN functions in this bisphenol-F phenolic precursor mixture. The PT-15 monomer mixture, represented by the single generalized structure **6**, is a multifunctional, low-viscosity (35 cps at 80 °C) liquid cyanate ester resin. PT-15 is cured via a thermally driven cyclotrimerization to form triazine rings, each of which serves as a cross-linking site. This reaction can take place readily in the absence of catalyst at temperatures above 165 °C.

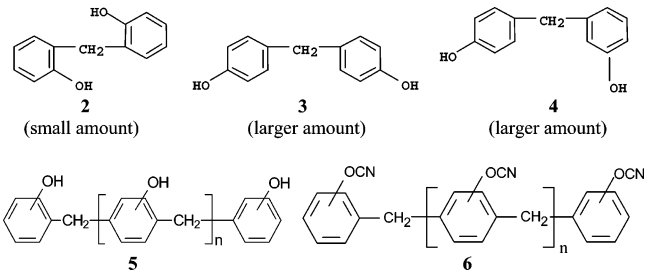

Multifunctional POSS, TriSilanolPhenyl-POSS, **1** ($C_{42}H_{38}O_{12}Si_7$, MW = 931.34 g/mol), with three SiOH groups, was purchased from Hybrid Plastics Inc.

Preparation of Composites. PT-15/POSS composites were prepared by a direct blending process. PT-15 (9.9, 9.7, 9.5, 9.0, or 8.5 g, respectively) was heated to 120 °C (η = 8 cps) and held for 10 min while stirring magnetically. Then, TriSilanolPhenyl-POSS-**1** (0.1, 0.3, 0.5, 1.0, or 1.5 g, respectively) was added as a powder into the low-viscosity liquid resin. These mixtures (total weight 10 g) were magnetically stirred for 50 min, during which time no viscosity increase occurred. POSS-**1** appeared to completely dissolve in each case into the clear, transparent PT-15 liquid. These solutions were placed into a mold without degassing and each sample was oven-cured. The cure protocol was as follows: heat to 188 °C and hold for 120 min, and then the temperature was ramped to 250 °C at 5 °C/min and held at 250 °C for 180 min. Each sample was then postcured at 300 °C for 30 min.

Measurements. The Fourier transform infrared spectroscopy (FTIR) measurements were conducted on a MIDAC Co. instrument at room temperature with 4 cm^{-1} spectral resolution by averaging 1024 scans. Cured samples were ground with KBr and pressed into pellets for measurement. Granulated specimens (∼1.0 g) of every composite were immersed into a large excess of THF at room temperature for 6 months to see if any POSS could be extracted by THF. Soxhlet extraction for 24 h in THF was also performed for each ground sample. Extraction of **1** would indicate that the extracted POSS was not chemically bonded into the resin matrix. After extraction, the THF solutions were concentrated and coated onto KBr plates and THF was removed for FTIR analysis of residue.

X-ray diffraction (XRD) measurements were performed to examine potential POSS alteration of solid-state polymer microstructure in the PT-15/**1** composites and to see if ordered (crystalline) POSS-**1** aggregates form by phase separation. Samples were examined using a Philips XPERT model X-ray diffractometer. Philips Analytical software and Cu Kα radiation (40 kV, 45 mA) were employed. Scans were taken over the 2θ range of 1−30° with a step size of 0.03° at 1 s/step.

Small-angle neutron scattering (SANS) experiments were performed at room temperature over the q range from 0.0038 to 0.2838 $Å^{-1}$ using the 30 m SANS instrument (NG7) at the National Institute of Standards and Technology (NIST) Center for Neutron Research (NCNR). The incident neutron wavelength was λ = 6 Å and the intensity at the sample was 17679 counts/s. The cross-sectional area of the beam was 50 mm × 50 mm and the entire cross section of the beam passed through the samples. The samples (100 mm diameters) were all solids. The scattered neutron intensities were corrected for background to yield the scattered intensities, $I(q)$, as a function of the wave vector, q, where $q = (4\pi/\lambda)\sin(\theta/2)$

(28) Grigat, E.; Putter, R. *Angew. Chem., Int. Ed. Engl.* **1967**, *6*, 206.
(29) Shimp, D. A.; Christenson, J. R.; Ising, S. J. *AroCy Cyanate Ester Resins: Chemistry, Properties and Applications*; Rhone-Poulenc Inc.: Louisville, 1991.

Scheme 1. Cross-linked Network Formation through Triazine Ring Formation

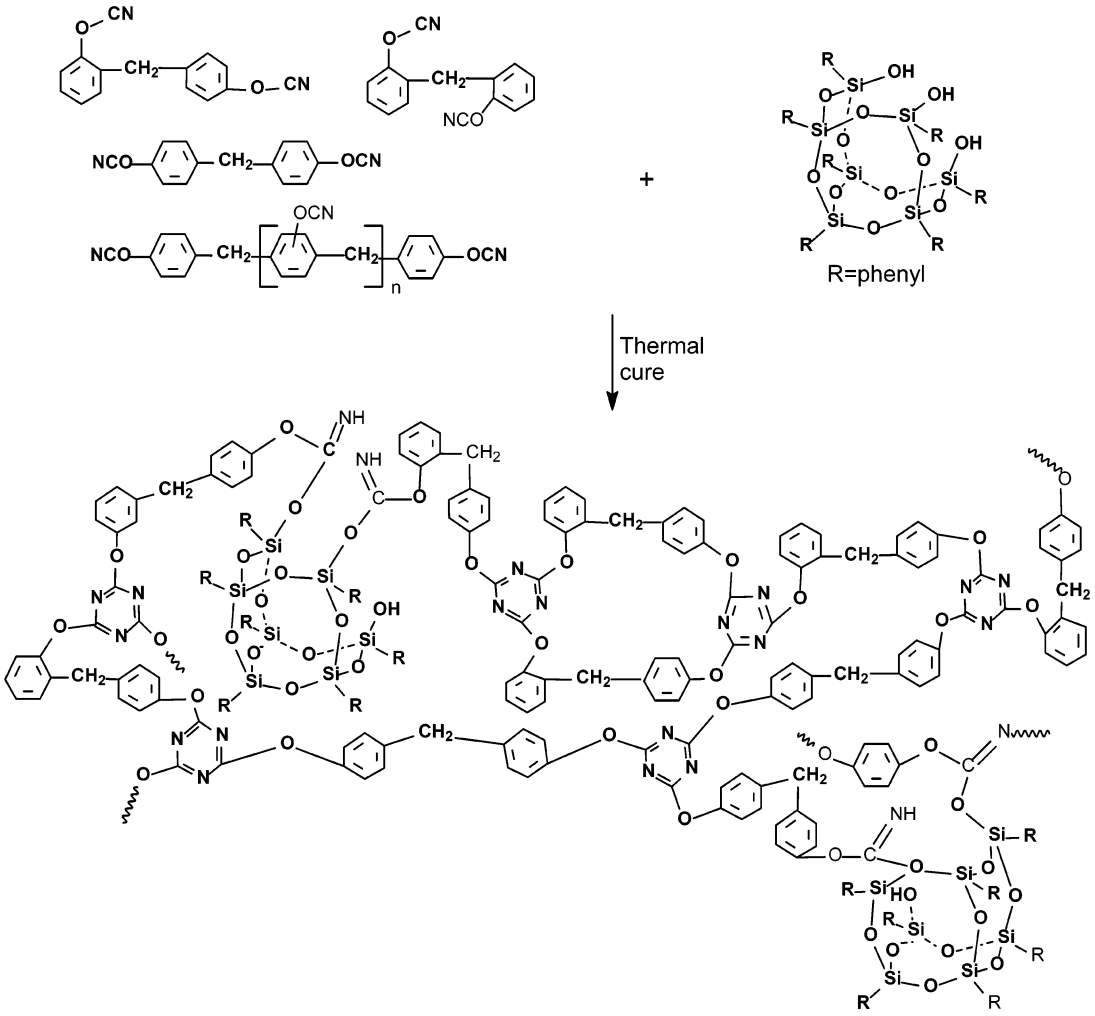

(θ is the scattering angle). IGOR software from WaveMetrics was employed for SANS data reduction.

A JSM-6500F field emission scanning electron microscope (FESEM) (JEOL USA Inc.) with an attached X-ray energy dispersive spectrometer (X-EDS) was used to obtain elemental compositions of the aggregated particles in PT-15/POSS composites and to examine the fracture surfaces after three-point bending flexural tests of neat PT-15 and PT-15/POSS composites. The samples for SEM were coated with gold before SEM measurements. The electron beam spot size used in X-EDS is about 5 nm in diameter.

Transmission electron microscopy (TEM) was used to identify and characterize phase separation of **1** in these composites. A JEOL JEM-2010 analytical transmission electron microscope (JEOL USA Inc.), located at Texas A&M University, operating at 200 kV with a measured point-to-point resolution of 0.23 nm, was used to characterize the phase morphology in the PT-15/POSS composites. TEM samples were ultramicrotomed to ~60−80 nm thicknesses and mounted on carbon-coated Cu TEM grids. The JEM-2010 instrument was equipped with an energy dispersive X-ray spectroscopy (X-EDS) system with an electron beam spot size of ~2 nm.

The dynamic storage moduli E' and loss factors (tan δ) were determined in the bending mode using a Rheometrics Scientific Model MK III DMTA instrument. A dual-level bending mode was employed. Small amplitude bending oscillations (both 1 and 10 Hz) were used at a gap setting of 8.00 mm. Measurements were carried out from 35 to 350 °C on each composite. PT-15/POSS test samples were approximately 3.0−4.0 mm thick, 4.5−5.5 wide, and 38 mm long.

Flexural strengths and flexural moduli were determined by three-point bending according to ASTM D-790-92 using a Zwick materials testing machine (model 1435) on 38 mm (length) × 10 mm (width) × 3−4 mm (thick) specimens. The flexural strength (FS) value was calculated at specimen failure according to eq 1:

$$\mathrm{FS} = \frac{3PL}{2Wt^2} \tag{1}$$

where P is the breaking force of the specimen, L the support span, W the width, and t the thickness. The flexural modulus (FM) was calculated from the tangent to the steepest initial straight-line portion of the load-deflection curve and using eq 2:

$$\mathrm{FM} = \frac{L^3M}{4Wt^3} \tag{2}$$

where L is the support span, M the tangent of the initial straight-line portion of the load-deflection curve, W the width, and t the thickness.

Results and Discussion

Reaction of PT-15 and TriSilanolPhenyl-POSS. Themal curing of PT-15 generates solid, cross-linked resins via cyclotrimerization of the OCN functions. This process forms

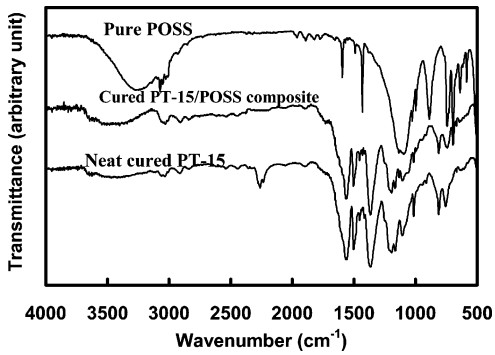

Figure 1. FTIR spectra of TriSilanolPhenyl-POSS, **1**, neat cured PT-15, and a cured PT-(15/**1** 85/15) w/w composite.

trisubstituted triazine rings. The triazine rings serve as thermally stable cross-linking hubs throughout the resin. In the presence of **1**, what reactions occur between cyanate esters and **1**? Cyanate esters form addition compounds with phenols, alcohols, amines, and most other labile hydrogen compounds upon heating or in the presence of base catalysts.[28] Amines add across cyanate esters at room temperature,[30] but phenol requires higher temperatures (100 °C) for rapid reaction.[31] These addition products are known to be important catalytic intermediates during triazine ring formation.[29] Thus, the silanol hydroxyl groups of **1** can also add across the CN triple bond of the cyanate ester groups of PT-15[29] as shown in Scheme 1 but they are less nucleophilic than phenol and require a higher temperature.

FTIR confirmed a reaction proceeded during curing between the silanol hydroxyl groups of **1** and OCN functions of PT-15. Figure 1 shows the FTIR spectra for pure **1**, neat cured PT-15, and its PT-15/**1** (85/15 w/w) composite. POSS-**1** exhibits a very broad band centered at ~3248 cm^{-1}, assigned to the stretching vibration of the hydrogen-bonded hydroxyl groups (O_3Si-OH) of **1**. Aromatic C−H stretching appears at ~3069 cm^{-1}. A strong Si−O−Si symmetric stretching peak appears at ~1100 cm^{-1} together with a sharp Si−O stretching vibration at ~1028 cm^{-1} for SiOH groups.[32] In the PT-15/**1** (85/15 w/w) composite, the stretching of the Si−OH groups is significantly decreased and the hydrogen-bonded hydroxyl group stretching peaks became indiscernible. The Si−O−Si symmetric stretching peak at ~1100 cm^{-1} was present. Moreover, a new N−H in-plane bending peak appeared at ~1570 cm^{-1}.[33] This peak together with the tris-oxygen-substituted triazine ring breathing vibration at ~1560 cm^{-1} appear (Figure 2).

Figures 3 and 4 show FTIR spectra of neat PT-15 and a PT-15/**1** (85/15 w/w) composite, respectively, after incremental stepwise curing at different temperatures. The gradual disappearance of −OCN peaks at 2240 and 2270 cm^{-1} and the appearances of absorptions at 1365 and 1565 cm^{-1} for triazine rings were observed. The intensity ratio of OCN (I_{OCN}, at 2240 and 2270 cm^{-1}) to the phenyl ring symmetric

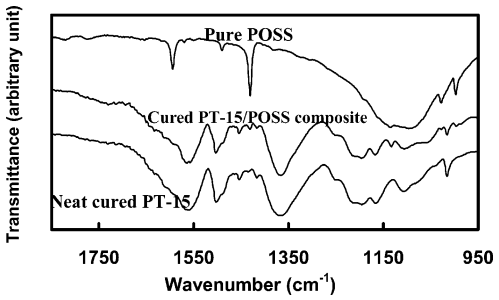

Figure 2. FTIR spectra of TriSilanolPhenyl-POSS, **1**, neat cured PT-15, and its PT-15/**1** (85/15 w/w) composite from 1850 to 950 cm^{-1}.

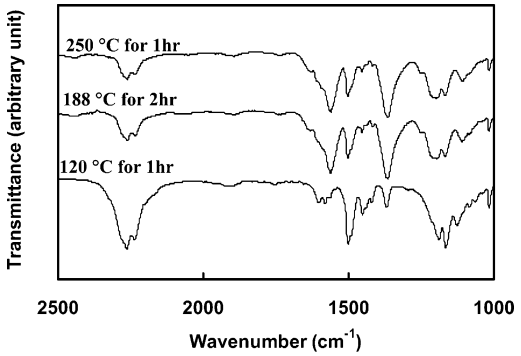

Figure 3. FTIR spectra from 2500 to 1000 cm^{-1} of neat PT-15 cured to different stages.

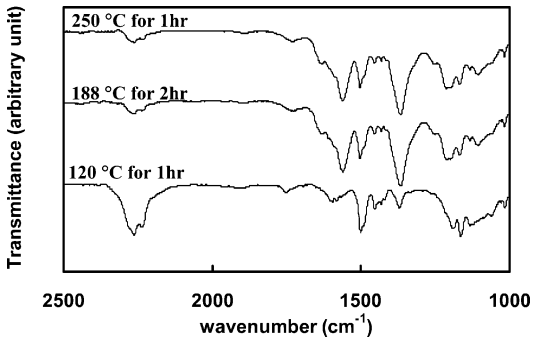

Figure 4. FTIR spectra from 2500 to 1000 cm^{-1} of PT-15/**1** (85/15 w/w) composite cured to different stages.

breathing vibration (I_{phenyl}, at 1500 cm^{-1}) decreases more quickly for PT-15/**1** composite than for pure PT-15 when held at 120 or 188 °C. The −OCN functions in PT-15 can either cyclotrimerize to form triazine rings or react by adding SiOH functional groups of **1** across the triple bond. Since phenyl rings do not participate in the reaction of triazine ring formation, the more rapid reduction of this I_{OCN}/I_{phenyl} ratio in the PT-15/**1** solutions must result from the additional addition reaction of SiOH across the −OCN functions. This addition is illustrated in Scheme 1.

Further evidence for this reaction is the appearance of a hydrogen-bonded imine stretching band in the FTIR spectra. Figure 5 shows FTIR spectra from 1630 to 1530 cm^{-1} of neat PT-15 and of the PT-15/**1** composite after each was heated at 120 °C for 1 h. A new absorption appeared at about 1595 cm^{-1}, which is due to the formation of the new C═N bonds by this SiOH addition in the PT-15/**1** solution. The absorption of iminocarbonate groups, $(RO)_2C{=}NH$, usually appears at 1640 cm^{-1}.[31] However, the (≡SiO)(RO)C═NH functions generated at 120 °C in the liquid state would be hydrogen-bonded to other C═NH functions or to other SiOH

(30) Liang, K.; Toghiani, H.; Li, G.; Pittman, C. P. *J. Polym. Sci., Part A: Polym. Chem.* **2005**, *43*, 3887−3898.
(31) Iijima, T.; Katsurayama, S.; Fukuda, W.; Tomoi, M. *J. Appl. Polym. Sci.* **2000**, *76*, 208−219.
(32) Liu, H.; Zheng, S.; Nie, K. *Macromolecules* **2005**, *38*, 5088−5097.
(33) Choi, J.; Harcup, J.; Yee, A. F.; Zhu, Q.; Laine, R. M. *J. Am. Chem. Soc.* **2001**, *123*, 11420−11430.

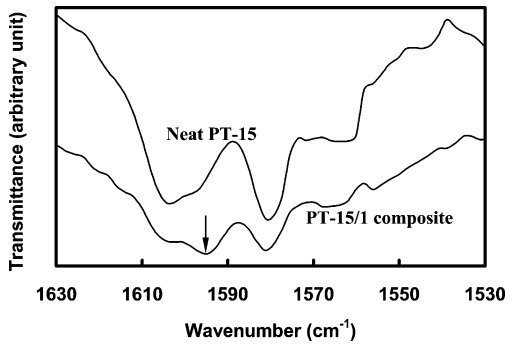

Figure 5. FTIR spectra from 1630 to 1530 cm^{-1} of neat PT-15 and its PT-15/**1** (85/15 w/w) composite after holding both for 1 h at 120 °C.

groups of **1** prior to extensive resin curing. This would shift this absorption to a lower frequency, which we observe at 1595 cm^{-1}. This is similar to the 35 cm^{-1} lowering of the IR absorption of the C═N bond in −ArO(O═P)C═NH when it becomes hydrogen-bonded.[34]

All samples were ground into powders and immersed in THF for 6 months to dissolve and extract oligomeric and linear polymeric components and any unreacted **1**. Each ground sample was also Soxhlet-extracted for 24 h in THF. **1** was not detected in the residues isolated by extracting these powdered samples of the PT-15/ **1** 99/1, 97/3, and 95/5 composites and then evaporating the THF after filtering. The FTIR spectra of **1** has a strong Si−O−Si symmetric stretching peak at ∼1100 cm^{-1} and a sharp Si−O stretching vibration (SiOH groups) at ∼1030 cm^{-1}. These bands were not present in the extracted residues from the PT-15/**1** (99/1, 97/3, or 95/5 wt/ wt) composites. Furthermore, only traces of a Si−O−Si symmetric stretching peak at ∼1100 cm^{-1} was detected in the residues isolated by extracting powdered samples of the PT-15/**1** 90/10 and 85/15 composites with THF. These FTIR results are consistent with chemical incorporation of **1** into the matrix as proposed in Scheme 1. Silanol functions add across the cyanate ester triple bond when the temperature is raised to 120 °C and above. Triazine ring formation proceeds above 150−160 °C. Scheme 1 presents a reasonable representation of the resin's structure. However, further increases in temperature to 250−300 °C must induce other changes in the structure. It increases cross-link density and likely causes further reactions at the imine functions in the composite.

Blending POSS-1 with PT-15. POSS-**1** exhibited good solubility in PT-15 at 120 °C and PT-15/1 99/1, 97/3, 95/5, and 90/10 liquid mixtures were transparent. The good solubility was due to the formation of specific intermolecular interactions (e.g., hydrogen bonding, −Si−OH···N≡C−O−) and phenyl ring π-interactions between **1** and PT-15. After the temperature was held at 188 °C for 120 min, all of these partially cured mixtures were still transparent. When the oven temperature was ramped to 250 °C at 5 °C/min and held at 250 °C for 180 min, PT-15/1 99/1, 97/3, and 95/5 composites remained transparent. However, the PT-15/1 90/10 composite became translucent, suggesting a dispersed phase formed with phase domain dimensions equal to or greater than visible light wavelengths. X-ray diffraction measurements were performed to try to detect (1) any alteration of solid state order in the PT-15 cured resin's microstructure and (2) to see if ordered POSS aggregates form by phase separation.

(34) Lin, C. H. *Polymer* **2004**, 7911−7926.

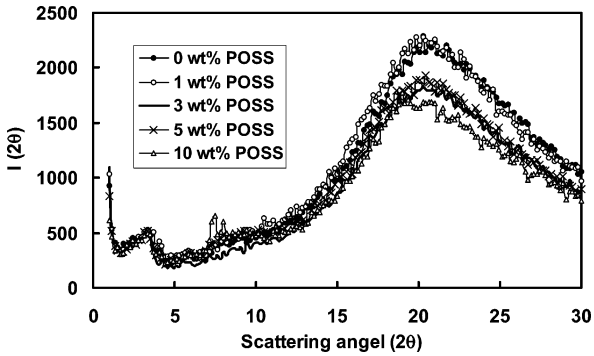

Figure 6. X-ray diffraction patterns of neat cured PT-15 resin and its PT-15/**1** 99/1, 97/3, 95/5, and 90/10 w/w composites.

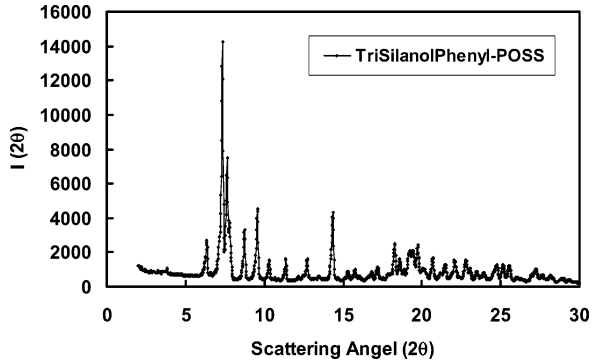

Figure 7. X-ray diffraction pattern of TriSilanolPhenyl-POSS, **1**.

Wide-Angle X-ray Diffraction (WAXD). The WAXD patterns for the cured PT-15 and the PT-15/**1** composites with w/w compositions of 99/1, 97/3, 95/5, and 90/10, respectively, are displayed in Figure 6. Figure 7 shows the wide-angle X-ray diffraction pattern for as-received **1**. One broad peak was observed at $2\theta \approx 20°$ in the WAXD pattern of neat PT-15. This broad peak is attributed to cured amorphous PT-15. The XRD patterns for the PT-15/**1** (99/1, 97/3, and 95/5) samples were essentially the same as that for the cured pure PT-15 sample. Thus, after curing, no specific evidence was found for aggregation of POSS-**1** into particles having a regular crystalline structural organization at loadings of **1** up to 5 wt %. In Figure 3, however, a small peak at $2\theta \approx 7.5°$ (equivalent to an interplanar spacing of 1.18 nm) is observed for the PT-15/**1** (90/10) composite. This peak corresponds to the distance between the TriSilanol-Phenyl-POSS moieties found in the pure solid sample of **1**. Thus, some aggregation of **1** into ordered particles must have occurred in this highly loaded PT-15/**1** (90/10) sample.

The solubility of **1** decreases during the cure, due to a smaller contribution by the positive entropy of mixing. However, substantial reaction of **1** with the resin has also occurred. When 10 wt % of **1** is present, aggregation and particle formation occurs due to phase separation which begins to occur at some point during the curing. The amount of solid **1** present and its degree of ordering in this sample is just sufficient for its XRD peak at 7.5° (2θ) to be observed. Some regular structure occurs within some POSS aggregates which are present in these phase-separated PT-15/ **1** (90/10) composites. The absence of any observable peak at 7.5° (2θ)

suggests that there is very little or no aggregation of **1** in PT-15/**1** (99/1, 97/3, and 95/5) composites. If aggregation occurs, it incorporates significant amounts of cyanate ester resin. In other words, molecular dispersion or formation of small unstructured diffuse aggregates of **1**, or a combination of both, was achieved in these 99/1, 97/3, and 95/5 composites (see SANS studies).

The X-ray diffraction pattern of the PT-15/**1** (99/1) composite overlaps exactly that of neat PT-15. Thus, the crystallographic structure of PT-15 does not change appreciably by adding only 1 wt % of **1**. On the other hand, the intensity of the peak at 20° (2θ) decreases and gradually shifts to a slightly smaller angle (about 19° (2θ)) upon adding more **1** into the PT-15 resin matrix. This peak shift corresponds to a progressive microstructural modification in the PT-15 resin matrix structure as the wt % of **1** increases from 3 to 5 to 10%. This changes the average layer spacing of PT-15 resin from 0.45 to 0.47 nm.

Small-Angle Neutron Scattering (SANS). Small-angle neutron scattering (SANS) is an excellent tool to analyze the size and dispersion of particles in a continuous medium.[35] The detection range of the NG7 30 m SANS instrument at the National Institute of Standards and Technology (NIST) Center for Neutron Research (NCNR) approaches 1 nm. This is about the size of a single POSS particle size ~1 nm in diameter if one includes the first atoms attached to each corner Si.

In a neutron scattering, the scattered intensity depends on the scattering length of the components forming the system, their concentration, and their relative positions in the sample.[35c,36] The coherent contribution to the scattered intensity, $I(q)$, from a two-component system with a particle volume fraction of ø and a single particle volume of V_p is proportional to the differential cross section per unit volume of the sample, $d\Sigma/d\Omega$ (cm^{-1}).[37] This term is given by

$$d\Sigma/d\Omega = b^2 \text{ø} V_p F(q) S(q)$$

with

$$b = (b_1 - b_2(v_1/v_2))$$

where b_1 and b_2 are the scattering lengths of components 1 and 2. The v_1 and v_2 terms are the monomer volume of the matrix polymer (component 1) and the molecular volume of the second component, respectively. This equation expresses the total coherent scattering in terms of a single particle form factor, $F(q)$, and the structure factor, $S(q)$, which accounts for interparticle interference. The scattering contrast in PT-15/**1** composites comes from the difference between the scattering lengths of the polymer matrix and the POSS-**1** particles. Structure factor, $S(q)$, is the Fourier transform of the correlation function of the mass center of the POSS particles. Thus, the SANS measurements give the Fourier transform of the POSS density.

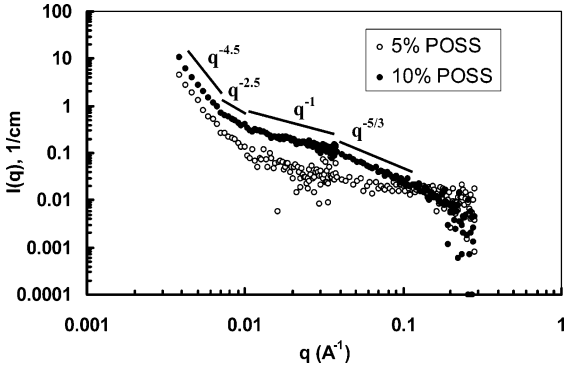

Figure 8. SANS profiles of PT-15/**1** 95/5 and 90/10 w/w composites.

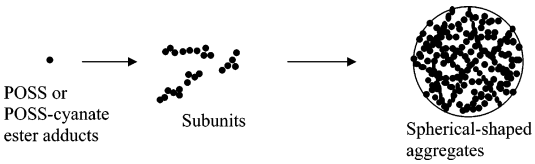

Figure 9. Schematic representation of formation of POSS-enriched aggregated regions.

Figure 8 displays sample SANS scattering profiles of PT-15/**1** 95/5 and 90/10 w/w composites. The slopes of the SANS profiles of 95/5 and 90/10 composites were not constant over the experimental q range. The scattering intensity of the 90/10 sample was higher than that from the 95/5 sample. The scattering curves were analyzed according to the ranges of q values, starting from 0.1 $Å^{-1}$, which corresponds to intraparticle dimensions (a few nanometers), and ends at 0.0038 $Å^{-1}$, which corresponds to the large-scale organization of about 165 nm.

At q values between 0.1 and 0.04 $Å^{-1}$, the scattering intensities of the 95/5 sample display a plateau. The plateau's intensity indicates there is little density fluctuation between 63 and 160 Å. Thus, the number density of particles (from 63 to 160 Å diameters) is similar over this length scale.[38] The scattering intensities from the 90/10 sample follow a $q^{-5/3}$ power law, where an exponent of −5/3 is indicative for swollen single chains.[39]

Between 0.04 and 0.01 $Å^{-1}$, the scattering intensities of both samples (5 and 10 wt % **1**) follow q^{-1} power law. An exponent with a value of −1 corresponds to the scattering from rodlike structures[39] or aggregates that are very tenuous or even stringy.[38] The q^{-1} power law over 0.04 and 0.01 $Å^{-1}$ implies that some molecules of **1** aggregate to form nano-rod-like domain diameters from 160 to 600 Å.

Between 0.01 and 0.007 $Å^{-1}$, the scattering intensity exponents of both the 5 and 10 wt % POSS-**1** samples change

(35) (a) Yoo, J. N.; Sperling, L. H.; Glinka, C. J.; Klein, A. *Macromolecules* **1990**, *23*, 3962−3967. (b) Yoo, J. N.; Sperling, L. H.; Glinka, C. J.; Klein, A. *Macromolecules* **1991**, *24*, 2868−2876. (c) Hanley, H. J. M.; Muzny, C. D.; Ho, D. L.; Glinka, C. J.; Manias, E. *Int. J. Thermophys.* **2001**, *22*, 1435−1448. (d) Ho, D. L.; Briber, R. M.; Glinka, C. J. *Chem. Mater.* **2001**, *13*, 1923−1931. (e) Ho, D. L.; Glinka, C. J. *Chem. Mater.* **2003**, *15*, 1309−1312. (f) Hanley, H. J. M.; Muzny, C. D.; Ho, D. L.; Glinka, C. J. *Langmuir* **2003**, *19*, 5575−5580.

(36) (a) Chen, S. H.; Lin, T. S. *Methods in Experimental Physics, vol. 23, Part B. Neutron Scattering*; Price, D. L., Skold, K., Eds.; Academic Press: London, 1987. (b) Higgins, J. S.; Benoit, H. C. *Polymers and Neutron Scattering*; Clarendon Press: Oxford, 1994. (c) Lin, Y.; Alexandridis, P. *J. Phys. Chem. B* **2002**, *106*, 12124−12132.

(37) Berriot, J.; Montes, H.; Martin, F.; Mauger, M.; Pyckhout-Hintzen, W.; Meier, G.; Frielinghaus, H. *Polymer* **2003**, *44*, 4909−4919.

(38) Pignon, F.; Magnin, a.; Piau, J.-M.; Cabane, B.; Linder, P.; Diat, O. *Phys. Rev.* **1997**, *56*, 3281−3289.

(39) Radulescu, A.; Mathers, R. T.; Coates, G. W.; Richter, D.; Fetters, L. J. *Macromolecules* **2004**, *37*, 6962−6971.

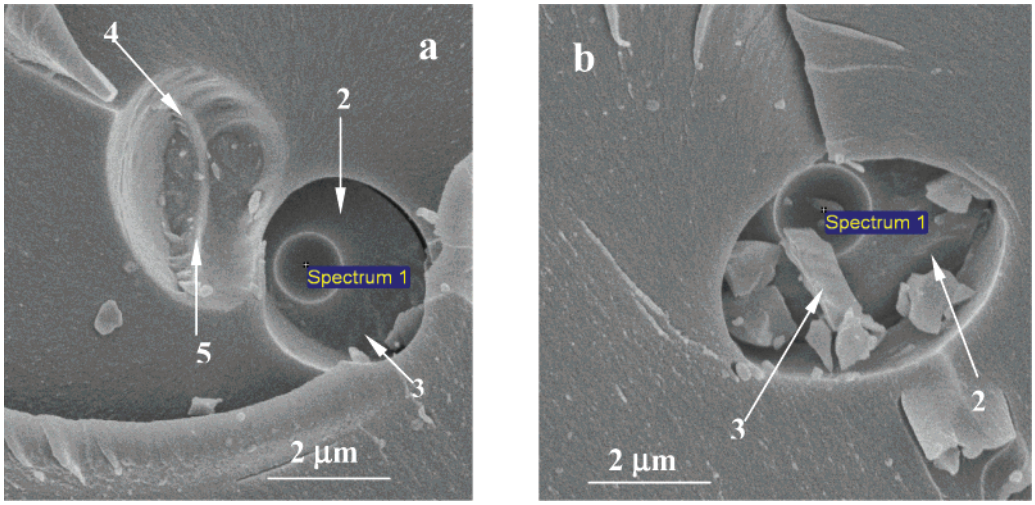

Figure 10. Two SEM micrographs of the PT-15/1 90/10 composite.

from −1 to −2.5, indicating some further aggregation to clusters 600−900 Å in size. Finally, at q values below 0.007 $Å^{-1}$, the scattering intensity exponents from both samples change from −2.5 to −4.5, indicating that aggregates with sizes >900 Å are present in both samples.

A slope of −2 indicates scattering from platelet shapes, while a slope of −4.5 is consistent with scattering from approximately spherical or from fractal-shaped clusters.[40] The exponent change of both 5 and 10 wt % samples can be explained by a two-step aggregation process: first, POSS molecules associate to form rodlike subunits with sizes ranging from 160 to 600 Å. Then these subunits associate to form larger aggregates with a more spherical shape (Figure 9). These aggregates do not have sufficient order to exhibit WAXD peaks in the 1, 3, or 5 wt % **1** samples and only register an extremely weak peak for the 10 wt % sample. Coughlin demonstrated that pendent POSS units present in ethylene-norbornylene-substituted POSS copolymers were found to aggregate and form elongated nonspherical lattices separate from crystalline polyethylene lattice regions.[41]

Scanning Electron Microscopy (SEM). Figure 10 displays two sample SEM micrographs of the translucent PT-15/**1** 90/10 composite. Table 1 summarizes the corresponding X-ray EDS elemental analysis of this composite at locations shown in Figure 10. Clearly, some POSS-**1** units have aggregated into approximately spherical POSS-rich particles at this high POSS-**1** loading. The numbers shown on the SEM micrographs refer to the EDS spectrum number represented in Figure 10. The heads of the arrows locate where the X-ray beams impinged on the sample. The spot size of the impinged X-ray beams were small (∼5 nm diameter) relative to the feature sizes observed in the SEMs. All of the regions studied exhibited the presence of **1** as indicated by the value of the silicon content. Pure **1** ($C_{42}H_{38}O_{12}Si_7$) contains 21.1 wt % and 7.07 atom % Si. The highest Si content exhibited by EDS spectrum 2 (Figure 10a.) contained only 12.13 wt % (2.56 atom %) Si, confirming that the POSS-rich phase-separated regions contain substantial amounts of PT-15 resin. This is further confirmed by their substantial nitrogen contents (from 9.89 to 13.16 wt % in Table 1.). Also, the weight percentages of POSS are different from point to point within the same POSS-rich domain. These findings are consistent with the very small XRD peak at 7.5° (2θ) in this 10 wt % **1** composite (Figure 6). The large aggregates cause the 10 wt % **1** sample to be translucent. The substantial PT-15 content within these aggregates is consistent with the clustering route proposed in Figure 9.

Table 1. X-ray EDS Spectra Data of PT-15/1 90/10 Composite (Figure 10)

spectrum	element	weight %	atomic %	POSS weight %
1a	C	68.85	74.10	
	N	11.72	10.81	
	O	17.68	14.29	
	Si	1.74	0.80	8.24
2a	C	65.56	71.27	
	N	13.16	12.27	
	O	18.71	15.27	
	Si	2.56	1.18	12.13
3a	C	70.22	74.92	
	N	11.45	10.48	
	O	18.08	14.48	
	Si	0.25	0.11	1.18
4a	C	66.72	72.31	
	N	12.93	12.01	
	O	17.84	14.51	
	Si	2.52	1.17	11.94
5a	C	68.79	74.15	
	N	12.13	11.21	
	O	16.79	13.59	
	Si	2.29	1.05	10.85
1b	C	71.01	76.18	
	N	9.89	9.10	
	O	17.18	13.84	
	Si	1.92	0.88	9.10
2b	C	69.40	74.51	
	N	12.08	11.12	
	O	16.91	13.63	
	Si	1.61	0.74	7.63
3b	C	68.90	73.88	
	N	12.83	11.79	
	O	17.18	13.83	
	Si	1.09	0.50	5.16

(40) Buckley, C. E.; Birnbaum, H. K.; Lin, J. S.; Spooner, S.; Bellmann, D.; Staron, P.; Udovic, T. J.; Hollar, E. *J. Appl. Crystallogr.* **2001**, *34*, 119−129.
(41) Zheng, L.; Waddon, A. J.; Farris, R. J.; Coughlin, E. B. *Macromolecules* **2002**, *35*, 2375−2379.

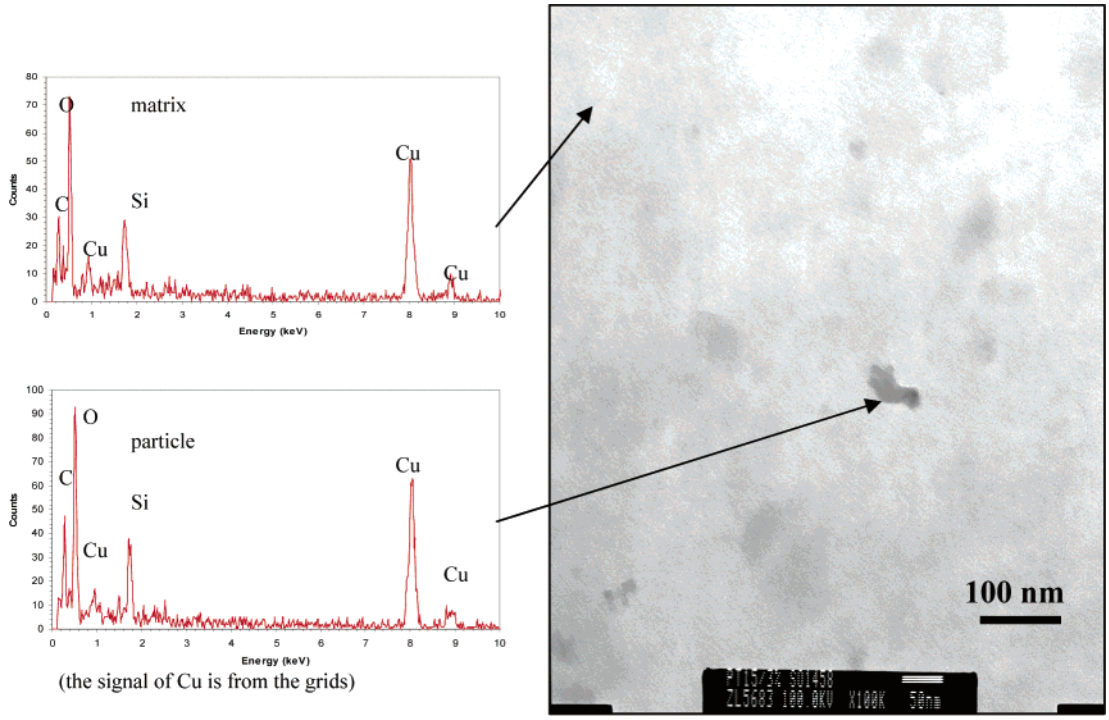

Figure 11. Progressive magnification TEM micrographs of the PT-15/POSS-**1** (97/3) composite showing molecular dispersion of **1** in PT-15. Si from molecules of **1** is dispersed in the resin matrix. The dark particle has the same Si/O/C composition as the resin matrix.

Transmission Electron Microscopy. PT-15/1 99/1, 97/3, and 95/5 composites were transparent. The 97/3 and 95/5 composite samples were selected for TEM measurements. Irregular regions appear in the TEMs of the nanocomposites (Figures 11 and 12), ranging from 200 nm to a few nanometers in diameter. The composition of these regions was studied by X-EDS and compared to the composition of what appears to be the continuous matrix regions.

X-EDS measurements detected substantial amounts of silicon in the continuous phase matrix of both the 97/3 and 95/5 samples. No silicon was found in cured samples of pure PT-15 resin. The regions of the 97/3 composite, which visually might appear to be particles in TEM micrographs, exhibit almost the same Si/O/C composition ratio as the continuous phase of the matrix (Figure 11). Thus, these darker regions may not really be POSS-rich aggregates. The "particle-like" inclusion or artifact in the 97/3 sample to which the arrow points (in Figure 11) has dimensions of about 50 × 25 nm. This feature exhibits the same Si/O/C composition within experimental error as the matrix region.

A TEM of the 95/5 composite is shown in Figure 12. With 5 wt % of POSS-**1** present, the observed particle-like inclusions were found to have a greater Si content than the surrounding matrix. The Si/O/C compositions varied for different particle (aggregate) regions in the 95/5 sample, but all of these domains contained a higher Si content than the continuous phase (Figure 12). Since the PT-15 resin itself does not contain any Si, the Si detected in the continuous matrix must be due to molecular level incorporation of **1** within the resin. This is consistent with a curing process that proceeds through the general chemical pathway shown in Scheme 1. The domains observed with higher Si contents than the matrix are best described as POSS-enriched aggregates because they do not contain as much Si as **1**. Thus, the appropriate interpretation is that some **1** has been dispersed molecularly within the matrix and the remainder forms aggregates which also incorporate various substantial amounts of resin. This means highly crystalline structures do not form, which agrees with the absence of XRD peaks for **1** in the 95/ 5 sample (Figure 6).

Various particles observed by TEM (Figures 11 and 12) could also have small amounts of matrix either above or below their boundaries, which is detected by X-EDS. This would also lead to different elemental ratios. However, the X-EDS spot size is very small (10 nm^2), giving confidence to the conclusion that the matrix is not being sampled within the plane of the micrograph because the particle areas studied by X-EDS are far larger than the X-ray beam. Thus, the TEM/X-EDS results augment the results from XRD and SEM/X-EDS. Each POSS-**1** core is surrounded by seven phenyl groups and contains three silanol (Si−OH) groups. Many POSS macromers are chemically bonded into the PT-15 resin. Aggregated regions, which also contain cyanate ester matrix components, are formed. These regions involve **1** that must be incorporated into the matrix since **1** cannot be extracted from these samples.

The TEM/X-EDS observations suggest that most POSS units are well-dispersed in the PT-15/**1** 97/3 and 95/5 samples. Two factors lead to the good dispersion of **1** in PT-15. First, **1** has a substantial solubility in uncured PT-15. This likely results from hydrogen bonding between the fairly acidic silanol OH groups and the nitrogen or oxygens of the cyanate ester functions. The seven phenyl rings of **1** can also be solvated by aryl rings in PT-15. Second, **1** is incorporated by chemical bonding into the developing PT-15 resin before and during curing as the composite forms. Thus, when the solubility limit of **1** was reached during curing, some **1** is already bound into cross-

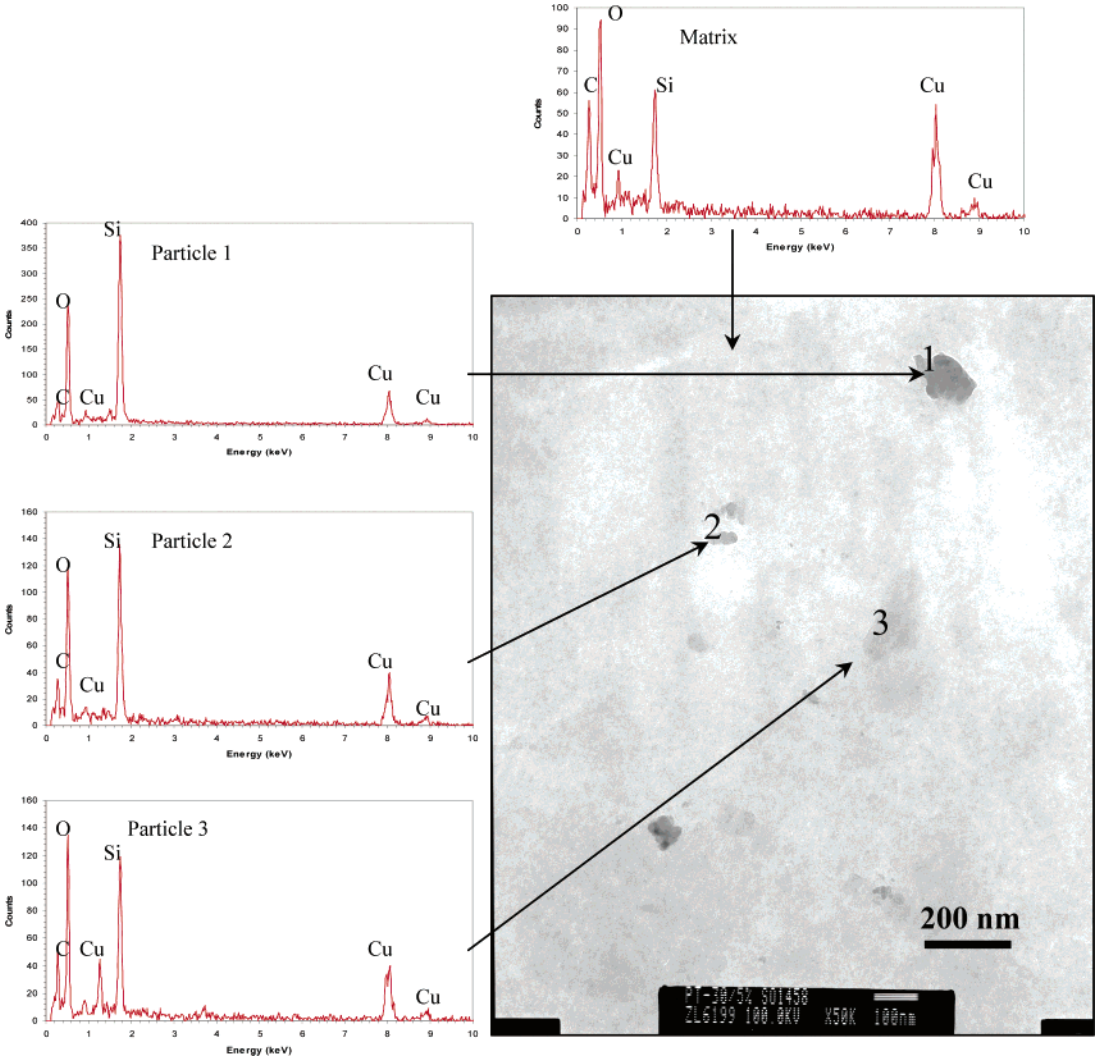

Figure 12. Higher magnification TEM micrographs of the PT-15/POSS-**1** (95/5) composite showing molecular dispersion of **1** in PT-15. Si is dispersed in the resin matrix. The particles have a higher Si content than the resin.

linked matrix regions and no longer free to self-aggregate. This limits the extent of phase separation. Furthermore, the concentration of unreacted **1** in the resin decreases as it reacts with the resin. As curing proceeds, the viscosity increases. This decreases the diffusion rates of **1**, thereby slowing aggregation. As cross-linking occurs, further aggregation of resin-bound **1** becomes more difficult.

In the 95/5 composite only small-sized (<200 nm) POSS-**1**-rich regions were formed. Some POSS-**1** could react with smaller cyanate ester molecules (monomers and oligomers) which are not yet cross-linked. A portion of these may aggregate, prior to further polymerization, which would then generate aggregates rich in POSS-**1** that contain cyanate ester which is chemically linked with the continuous matrix regions.

Mechanical Properties. *DMTA Studies.* The bending storage modulus, E', versus temperature curves at 1 Hz for neat PT-15 and each PT-15/**1** composite are shown in Figure 13. The E' (both above and below T_g) values of the 99/1, 97/3, and 95/5 composites are higher than those of the pure PT-15 over the entire 35−350 °C temperature range. These three composites also display T_g values ~15 to 25 °C higher than the T_g of the pure PT-15 prepared under identical

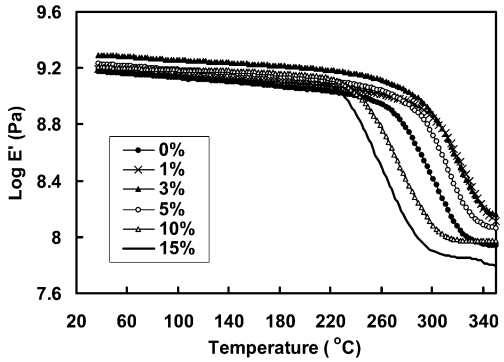

Figure 13. Bending modulus (E') versus temperature curves at 1 Hz (from DMTA) for neat PT-15 and its PT-15/**1** 99/1, 97/3, 95/5, 90/10, and 85/15 w/w composites.

conditions. Importantly, their E' values above T_g are significantly higher than that of the cured PT-15 resin. As the amount of **1** increases to 10 and 15 wt %, the T_g values drop as do the E' values at $T > T_g$. While PT-15/**1** 90/10 and 85/15 composites exhibit higher E' values than those of the pure PT-15 in the glassy region ($T < T_g$), the 15 wt % POSS-**1** sample exhibited lower E' values in the rubbery region ($T > T_g$). Furthermore, the T_g values are lowered by 25 and 35 °C in the 10 and 15 wt % POSS composites,

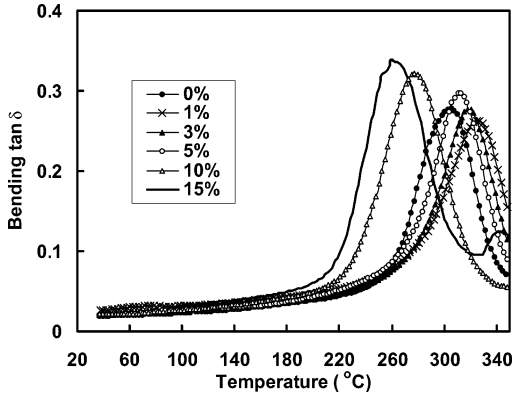

Figure 14. Bending tan δ versus temperature curves at 1 Hz (from DMTA) for neat PT-15 and its PT-15/**1** 99/1, 97/3, 95/5, 90/10, and 85/15 w/w composites.

respectively, versus pure PT-15. Thus, small amounts ($\leq$5 wt %) of **1** incorporated into PT-15 can increase the storage modulus in the glassy and rubbery regions and the T_g values versus pure PT-15. As the amount of **1** increases (10 and 15 wt %), the T_g and E' ($T > T_g$) values drop below that of the parent cyanate ester resin.

The bending tan δ versus temperature curves obtained at 1 Hz (from DMTA) for the pure PT-15 and the PT-15/**1** composites are shown in Figure 14. The T_g values for the PT-15 resin and its 99/1, 97/3, 95/5, 90/10, and 85/15 composites, defined as the tan δ peak temperatures, are 305, 325, 321, 313, 278, and 260 °C, respectively. The 99/1 sample has the highest T_g among these samples. The T_g values then decrease as the content of **1** increases.

Table 2. Flexural Strength (FS) and Flexural Moduli (FM) of PT-15/POSS Composites[a]

samples	FS (MPa)	FM (MPa)
PT-15	120.72	3337.78
PT-15/POSS 99/1	121.18	3385.99
PT-15/POSS 97/3	122.29	3832.38
PT-15/POSS 95/5	123.54	4267.73
PT-15/POSS 90/10	124.64	3634.95
PT-15/POSS 85/15	145.43	3558.28

[a] Six samples of each were averaged.

Two factors affect the viscoelastic properties. First, **1** is relatively rigid. Massive units of **1** along chain segment units will tend to retard or restrict that segment's motions in PT-15. However, **1** may also increase free volume by not packing as well overall with the cyanate ester resin segments of the cross-linked resin. The first factor increases both the rigidity and the T_g while the second adds free volume, lowers T_g, and could allow increased segmental motion. A portion of the three available acidic silanol (Si−OH) groups of **1** can be chemically bound into cured PT-15 (Scheme 1). Incorporating **1** may decrease the overall cross-linking density since the volume of each POSS-**1** molecule is substantial. This in turn could decrease T_g of the composite by lowering the cross-link density per unit volume. When the reduction of segmental motion dominates, then the rigidity and T_g of the composite will increase. However, at larger loadings of **1** the trend reverses. A lower net cross-link density and/or increased free volume is consistent with the increased flexural strength of the PT-15/**1** 85/15 w/w sample which could undergo greater bending (see flexural properties). Changes

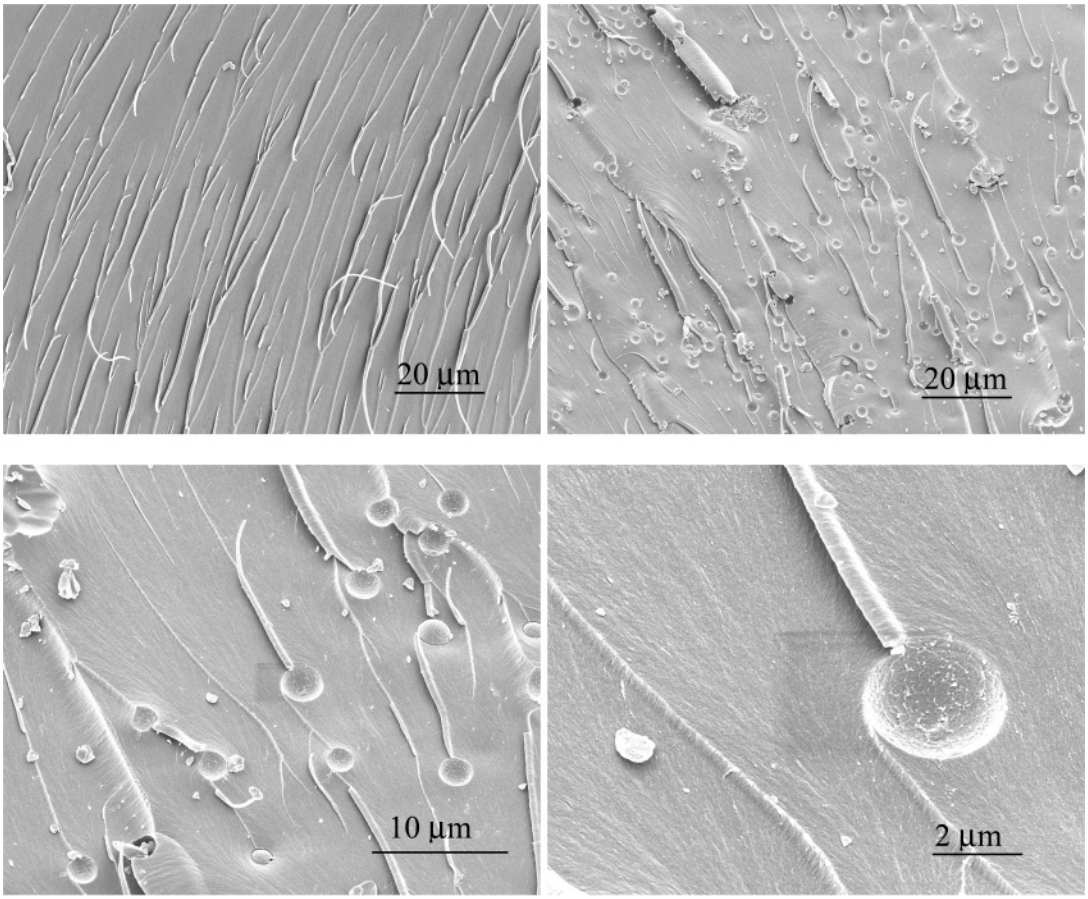

Figure 15. Fracture surface SEM micrographs: (a) neat PT-15 and (b−d) PT-15/**1** 85/15 w/w composite.

in the extent of aggregation and detailed morphology also occur as the content of **1** increases (≥10 wt %). Finally, as the loading of **1** goes up, the remaining acidic SiOH functions may modify the degree of triazine formation.

Flexural Properties and Fracture Surfaces. The flexural strengths and moduli of the PT-15/**1** composites are shown in Table 2. The flexural strengths of PT-15/**1** samples are slightly higher than that of neat PT-15 resin and increase as the loading of **1** increases. Only the PT-15/**1** 85/15 sample exhibits a sizable flexural strength improvement (20%). Also, the flexural moduli are higher than that of neat PT-15 resin. The flexural moduli increase as the content of **1** increases and then decrease as the wt % of **1** increases to 10 and 15%. The PT-15/**1** 95/5 sample exhibits the highest value, 28% above that of the neat PT-15 resin. Therefore, the mechanical properties of PT-15 resin can be improved by incorporation of **1**.

Fracture surface SEM micrographs of the neat PT-15 and the PT-15/**1** 85/15 w/w composite after failure in the three-point bend flexural test are shown in Figure 15. Crack propagation, as indicated by failure ridges, is straighter for the neat PT-15 resin (Figure 15a). In contrast, these failure ridges seem to interact with and terminate at POSS-rich aggregates during crack propagation within the PT-15/**1** (85/15) composite (Figures 15b−d). Some blunting of the failure process occurs. The aggregates also seem to act as crack attractors for a propagating crack front. Intermittent interruption of crack growth gives rise to a more complex crack propagation path instead of a relatively straight/smooth fracture path.

Conclusions

The liquid PT-15 cyanate ester resin dissolved **1**. After curing, FTIR, XRD, SANS, and X-EDS analyses indicated that a portion of **1** was molecularly dispersed and bonded into the continuous matrix phase, while some was present in aggregates and/or particles containing both **1** and cyanate ester resins. At 1 and 3 wt % POSS loadings, appreciable fractions of **1** are molecularly dispersed. SANS and TEM also detected POSS-enriched nanophases (from a few nanometers to about 200 nm) in the composites. These nanophases also incorporate cyanate ester. The size distribution of these phases broadens and larger aggregates increasingly form as the loading of **1** increases. At 15 wt % **1**, the dispersed particulate phase clearly influences the fracture mechanism. The storage moduli, E', of PT-15/**1** 99/1, 97/3, and 95/5 composites are higher than those of the pure cured PT-15 over the entire temperature range 35−350 °C. The E' values for all the composites (except that when 15 wt % of POSS was present) are greater than that of the pure resin at $T > T_g$. Also, the T_g values of the 1, 3, and 5 wt % POSS composites are higher than that of neat PT-15. Small amounts (≤5 wt %) of POSS can improve the storage modulus the most. The flexural strength and flexural modulus are higher than those of neat PT-15 and larger amounts of **1** (>3 wt %) are most beneficial.

The aggregation/phase separation process is quite complex. First, **1** chemically reacts with cyanate esters to form imino siloxycarbonates. This improves dispersion. Continued curing leads to aggregation of **1** which is bound to resin molecules. The aggregation process depends on the concentration of **1** used. Cross-linking eventually gels the system but as the temperature increases to 250 °C the fate of the imino siloxycarbonate functions is unknown. Some formation of SiOSi bonds from silanol groups of **1** may also occur, both intramolecularly and intermolecularly at 250−300 °C. The latter could create dimers or trimers of **1** when there is enough freedom of motion or when molecules of **1** are in close proximity.

Acknowledgment. The authors thank Z. P. Luo at Texas A&M University for obtaining the TEMs shown here. The authors acknowledge the support from the National Institute of Standards and Technology, U.S. Department of Commerce, for providing the neutron research facilities and funding (Proposal number S14-13, U14-02, Submission ID: 3456). Partial support was provided by the Air Force Office of Scientific Research STTR program (Contract No. F49620-02-c-0086 and Grant No. F49620-02-1-026-0).

CM051582S